Fabrication of Electrodeposited Ni–Fe Cantilevers for Magnetic MEMS Switch Applications

Giuseppe Schiavone, *Student Member, IEEE*, Andrew S. Bunting,
Marc P. Y. Desmulliez, *Senior Member, IEEE*, and
Anthony J. Walton, *Senior Member, IEEE*

***Abstract*— Electrodeposited alloys of nickel and iron are prone to suffer from the development of undesirable-stress gradients resulting from process steps and heat treatments following deposition. As a result, the yield associated with devices using permalloy (Ni–Fe, 80%–20%) films can be severely compromised. Although electrodeposition recipes have been formulated that greatly reduce stress in Ni–Fe films, any stress gradients through the thickness of permalloy can pose considerable problems during the release of cantilevers. The development of such gradients is typically the direct result of the selected design and process architecture and/or problematic material choices. This paper presents an improved architecture for electroplated Ni–Fe free-standing microcantilever structures. This architecture minimizes the development of stress gradients in cantilever beams and facilitates the use of suspended permalloy cantilever structures in magnetically actuated microelectromechanical systems (MEMS) switches. [2014-0170]**

***Index Terms*— Magnetic MEMS, microelectromechanical systems (MEMS) switches, permalloy, microactuators, stress gradient, electrodeposition, surface micromachining.**

I. Introduction

THE UNCONTROLLED development of stress in MEMS films can be detrimental for both device performance and reliability, and the particular problems associated with stress development in micromachined films are therefore of widespread interest [1]–[4]. Alloys of nickel and iron and in particular Permalloy (Ni-Fe, 80-20%) are important materials for the microfabrication of integrated passive magnetic devices [5]–[7] due to their high magnetic permeability and low coercivity [2], [8], [9]. However, Permalloy films typically exhibit high sensitivity to failure mechanisms induced by the relief of residual stress [10]–[12].

Manuscript received June 2, 2014; revised August 27, 2014; accepted September 2, 2014. Date of publication September 17, 2014; date of current version July 29, 2015. This work was supported in part by the Edinburgh Research Partnership in Engineering and Mathematics, University of Edinburgh, Edinburgh, U.K.; in part by the Engineering and Physical Sciences Research Council through the Innovative Electronics Manufacturing Research Centre under Grant DTA/15/2007 and Grant FS/01/02/10 within the Smart Microsystems Grant; and in part by Texas Instruments Inc. Subject Editor S. M. Spearing.

G. Schiavone, A. S. Bunting, and A. J. Walton are with the School of Engineering and Electronics, Institute of Integrated Micro and Nano Systems, University of Edinburgh, Edinburgh EH9 3JF, U.K. (e-mail: giu.schiavone@gmail.com; andrew.bunting@ed.ac.uk; anthony.walton@ed.ac.uk).

M. P. Y. Desmulliez is with the School of Engineering and Physical Sciences, Heriot-Watt University, Edinburgh EH14 4AS, U.K. (e-mail: m.desmulliez@hw.ac.uk).

Color versions of one or more of the figures in this paper are available online at http://ieeexplore.ieee.org.

Digital Object Identifier 10.1109/JMEMS.2014.2355214

Ni-Fe alloys find potential applications in the manufacture of microelectromechanical switches with magnetic actuation [13]–[21]. Magnetic architectures offer many advantages over other actuation schemes for MEMS switches, particularly electrostatic actuation. These benefits include long-range actuation forces, allowing for larger contact gaps and thus providing better isolation in the OFF-state, and greater robustness to stiction and other wear and failure mechanisms [22]. The need for high voltages to achieve electrostatic actuation is also alleviated, creating the opportunity to employ low-voltage electrostatic latching mechanisms. These can be applied subsequent to magnetic actuation for the retention of the switch state with near-zero power consumption (except for the charging energy). This combination enables the development of novel devices, which can offer greater performances in terms of OFF-state isolation, lower voltage actuation for compatibility with standard silicon integrated circuits, and lower power consumption, even when benchmarked against semiconductor switches if employed with high frequency signals [23].

Previous studies [24], [25] have reported process monitoring and control routines that have successfully enabled the electrodeposition of low-stress Ni-Fe on 200 mm silicon substrates. The deposition techniques described have a demonstrated capability to minimise the development of residual stress in both thick Ni-Fe blanket films (2 to 5 μm) and relatively simple patterned structures. However, more complex devices fabricated in such films can suffer from failures related to stress gradients which result from non-optimal design practices and material choices.

This paper presents an improved design for electroplated Ni-Fe freestanding microcantilever structures for use in magnetically actuated MEMS switches, with particular focus on the stress gradient developed within the patterned electrodeposits during surface micromachining. The stress problems encountered during the fabrication of such structures are first presented. An experimental plan is then devised to investigate the root cause of the development of stress gradient through the thickness of the ECD films, and a solution is finally proposed and demonstrated.

II. Micro Switch Devices

Following the work reported in [26], the viability of electroplated Ni-Fe freestanding cantilever structures for use in switching devices has been assessed by fabricating the actuating portion of a magnetic MEMS switch. The complete

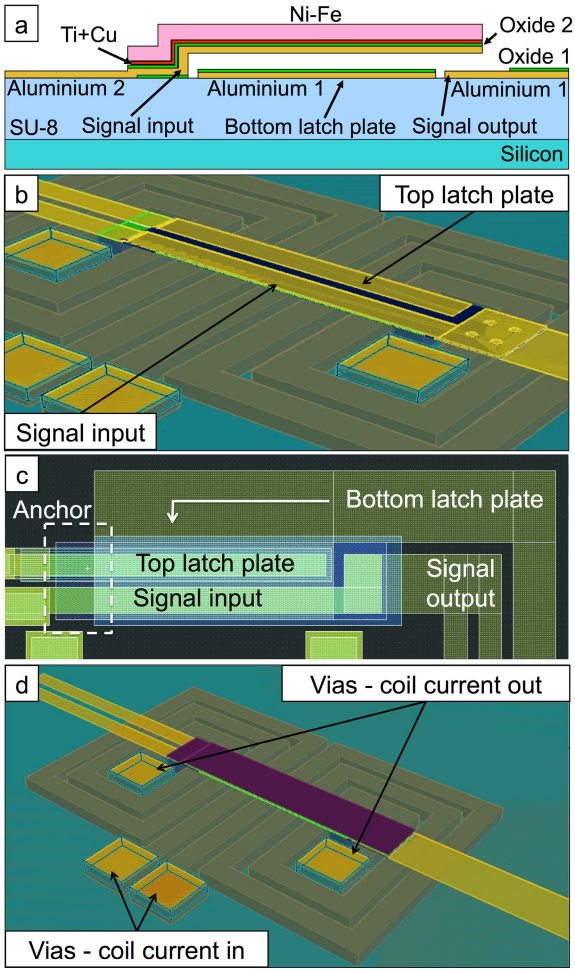

Fig. 1. (a) Cross section of the magnetic switch. (b) 3D view of the metal lines on the bottom surface of the cantilever (with the Ni-Fe cantilever removed). (c) Mask layout. (d) 3D view of complete switching device. The 3D schemes include embedded actuation coils for a complete switch. Note that the metallisation on the bottom surface of the cantilever defines two independent conduction lines for the switched signal and the electrostatic latch (b, c). Electrical access to the bottom latch plate is not shown in (d) for ease of visualisation.

device features planar coils for magnetic excitation and a switched conductive line composed of two parts: the signal input track that runs along the bottom surface of a Ni-Fe cantilever, and the signal output track located on the substrate. When magnetically actuated, the cantilever is attracted to the substrate and deflects downwards, closing the contact between the two signal lines (ohmic) or bringing them into close proximity (capacitive). To avoid a constant current being required in the coils to maintain the switch in the ON-state, an electrostatic mechanism is integrated that latches the cantilever down on the substrate. The excitation coils generate long-range magnetic forces that pull the cantilever down from a large gap. Once actuated, the bottom surface of the cantilever forms a capacitor with a metal-insulator stack on the substrate, which enables the structure to be electrostatically held in the ON-state with near-zero power consumption. Fig. 1 shows a cross-section and 3D views of the test device.

The first metal layer (Aluminium 1, Al 1) defines the output signal connection and the bottom electrostatic latch plate, with the second level metal (Aluminium 2, Al 2) defining the

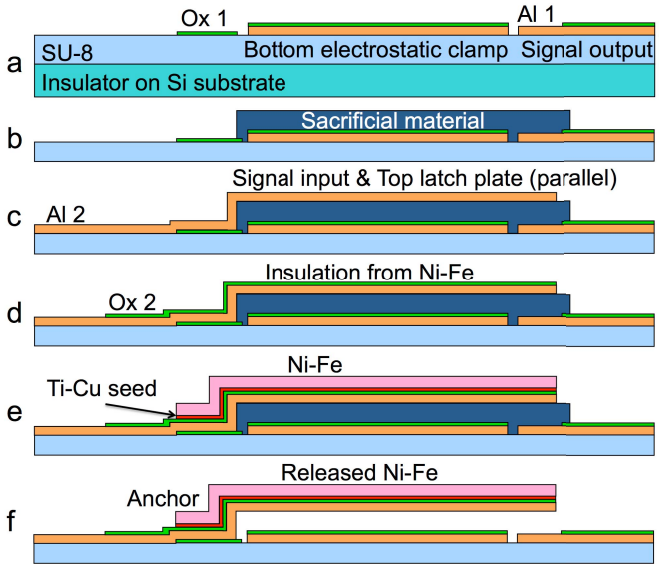

Fig. 2. Process flow for the fabrication of the MEMS switching test structures.

input signal connection and the top electrostatic latch plate. These run parallel to each other on the bottom surface of the cantilever (Fig. 1(b)). The fabrication of the test devices follows the process flow illustrated in Fig. 2.

Silicon wafers were processed by first depositing a 300 nm thick PECVD silicon oxide layer, followed by spin coating SU-8 to mimic the polymeric surface resulting from embedded actuation microcoils in the complete switch as illustrated in Fig. 1. SU-8 epoxy is one option along with other polymers that have been used as a structural dielectric in which to embed integrated coils [27]–[29]. The formulation used for this work was SU-8 3010 produced by MicroChem Corporation, spun at a thickness of approximately 19 μm and hard baked at 200 °C for 20 minutes.

The fabrication of the test devices starts with the deposition of the first metal layer, which is patterned to define the bottom capacitor plate for the latching mechanism and the output signal line. A blanket sputter deposition of 300 nm of Al is patterned by means of reactive ion etch (RIE) using a 1.2 μm thick positive photoresist mask (Megaposit SPR350). The bottom dielectric layer is then deposited to insulate the bottom latching plate and, in the case of capacitive switches, the output signal line. The following 200 nm thick SiO_2 dielectric layer is deposited using plasma enhanced chemical vapour deposition (PECVD). This is subsequently RIE patterned in fluorine plasma and Fig. 2(a) shows a cross-section of the cantilever at this stage of processing.

A sacrificial layer is then deposited and patterned to facilitate the release of the Ni-Fe cantilever. It is important to precisely control the thickness of this layer as it defines the actuation gap, set to a design specification of 2 μm. The patterned sacrificial mesas, Fig. 2(b), serve as a resting surface for the cantilever and the electrical lines for the signal input and the top capacitive plate for the electrostatic latch mechanism. The first candidate material investigated for this sacrificial layer was Parylene-C, which can be vapour deposited at room temperature, patterned by means of RIE, and completely removed in an O_2 plasma chamber.

TABLE I
Ni-Fe ELECTROPLATING BATH COMPOSITION

Component	Concentration (gL^{-1})
NiCl2·6H2O	110
$FeCl_2 \cdot 4H_2O$	8
H_3BO_3	25
Saccharin	1
Na dodecyl sulphate	0.1
HCl	5

A second aluminium deposition and patterning process defines the input signal line and the top capacitor plate for the electrostatic latching mechanism. The two tracks run from the insulating substrate onto the top surface of the sacrificial mesa, as shown in Fig. 2(c). A second PECVD SiO_2 layer is then patterned as shown in Fig. 2(d), which insulates the input signal line and the top capacitor plate from the Ni-Fe cantilever, in order to enable the two voltages to be set independently.

Once the electrical lines and insulating structures are patterned, the electrodeposition of the Ni-Fe cantilever completes the magnetic actuator. A bottom-up electrodeposition approach is used to define the structure that is anchored to the insulating substrate and runs up onto the sacrificial mesa. This process begins with the sputter deposition of a Ti and Cu bilayer on the substrate. Copper serves as seed layer for electroplating at an optimum thickness of 300 nm to ensure good conductivity over the entire area of the wafer, whereas the 30 nm thick titanium promotes adhesion between the copper and the underlying materials. Photolithography is then performed to define the electroplating areas using a positive photoresist mask. The electrodeposition of the Ni-Fe cantilevers is performed in a 35 L tank containing a solution prepared using the components and the quantities reported in Table I.

Based upon the results obtained from previously reported studies [24], a combination of mild agitation and low current density (10 mA cm^{-2}) is used to achieve a good compromise between thickness uniformity across the wafer surface, the desired Ni-Fe ratio and low residual stress. After electrodeposition, the photoresist mould is stripped and the exposed Ti and Cu seed layer is etched, as shown in Fig. 2(e).

The sacrificial mesa is finally completely removed to release the cantilever, which supports the metallisation and insulation on its bottom surface as illustrated in Fig. 2(f). The resulting freestanding structure is therefore a stack consisting of a metal and dielectric layer, a seed layer of 30 nm Ti and 300 nm Cu, and finally the 2 μm electroplated Ni-Fe cantilever, anchored to the bottom insulator layer.

Fig. 3 shows SEM micrographs of completed and released test devices with all features previously described.

Although the above process successfully produced working devices, the removal of Parylene-C proved to be a very time-consuming treatment requiring up to 2 hours in the RF chamber. Besides being inefficient, this process was detrimental to both Ni-Fe and the embedded SU-8 matrix, damaging many of the devices on the wafer and thereby significantly reducing the wafer yield. Fig. 4 illustrates two examples of completed test actuators where the Ni-Fe cantilevers have been damaged by the oxygen plasma treatment used to remove the sacrificial Parylene-C.

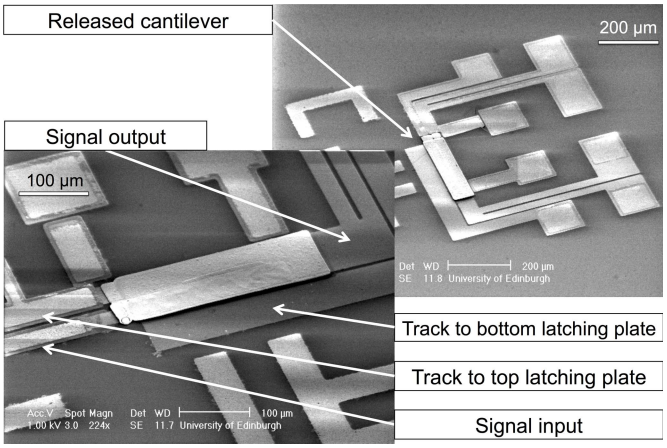

Fig. 3. SEM images of completed test devices with components identified.

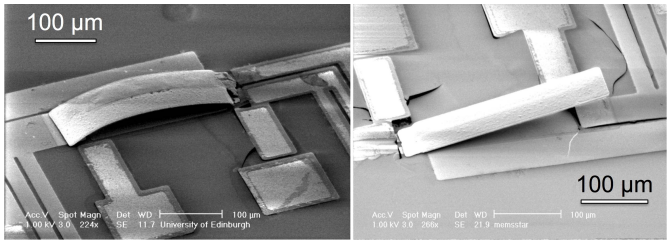

Fig. 4. SEM images of test devices deteriorated by the oxygen plasma sacrificial etch treatment. The devices do not show signs of release until treated in oxygen plasma for 1 or 2 hours, after which the top of the Ni-Fe is oxidised and the underlying SU-8 layer begins to crack.

The strategy used to implement a more effective etch release process was to produce a test chip expressly designed to investigate and enable the identification of the performance limits of the critical release step as well as evaluate different combinations of candidate sacrificial materials.

III. RELEASE TESTS

To characterise the release process, a set of low-resolution emulsion photomasks of test structures was designed with the purpose of identifying:

1) the minimum beam width that could be released;.
2) the possible need for etch-release holes (size and spacing);
3) the presence of stress gradient in the film thickness;
4) the amount of strain in Ni-Fe beams.

The test chip included the following structures, with a number of combinations of beam widths, anchor geometries and etch-release hole patterns.

1) Cantilever structures (200 μm and 300 μm long) with widths ranging from 20 μm to 100 μm, in steps of 10 μm with four different anchor geometries, as shown in Fig. 5(a-d). The purpose of these was to investigate their robustness to the surface micromachining process under investigation.

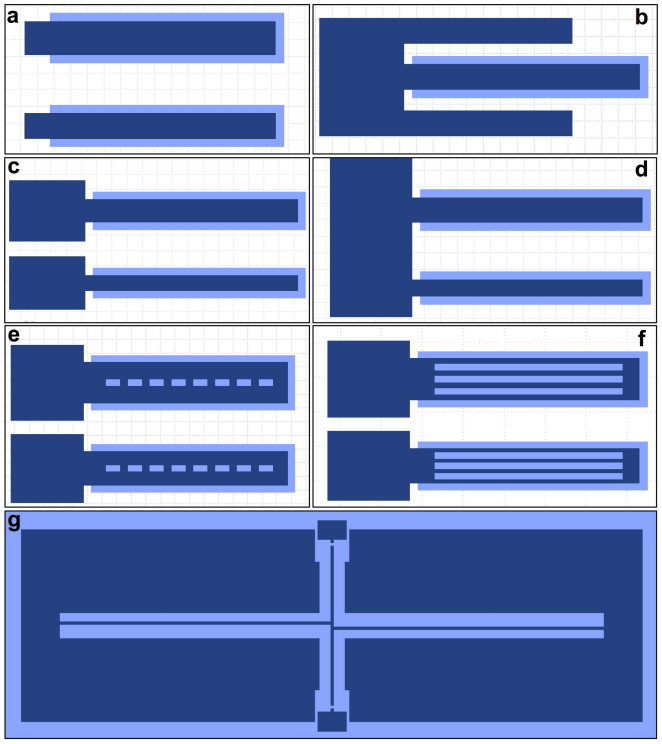

Fig. 5. Cantilever design variations for the investigation of the release process. The lighter layer is the sacrificial material, whereas the darker shaded layer is the ECD Ni-Fe. The beams shown are 300 μm long. Anchors of the same width as the cantilevers (a), wider protruding anchors (b), an anchor that expands on the sides to provide better stability (c), and a common anchor structure shared by a set of cantilevers of varying width (d) are included. Etch-release hole patterns are introduced to facilitate undercut during the dry etch release process: discrete holes distributed along the centreline of the beams (e), and series of 3 continuous slits distributed over the width of the beam (f). Rotating arm stress relief structure (2 mm $\times$ 0.6 mm) on the sacrificial layer for release (g).

2) Cantilevers were also designed with different etch-release hole patterns distributed on the beam layout, with the aim of reducing the degree of undercut required for the complete release. The chosen dimensions for the etch-release holes were (in μm): 10 $\times$ 20 with 10 μm separation, 10 $\times$ 10 with 20 μm separation, 1 $\times$ 230 as a single slit, 5 $\times$ 20 with 10 μm separation, 5 $\times$ 10 with 20 μm separation, 5 $\times$ 230 as a single slit, 2 $\times$ 20 with 10 μm separation, 2 $\times$ 10 with 20 μm separation, and 2 $\times$ 230 as a single slit. The holes are arranged in a single row (Fig. 5(e)), or over three rows spanning the whole cantilever width (Fig. 5(f)).
3) Suspended rotating test structures to monitor the strain [24], [25] were also included in the layout (Fig. 5(g)), with the aim of visually monitoring possible differences in the development of stress gradients.

Fig. 6 presents a cross-section of the process flow for the fabrication of the test cantilevers shown in Figure 5. This fabrication process requires the following steps. a) Preparation of the substrate by depositing 300 nm PECVD SiO_2. b) Blanket deposition of 2 μm thick sacrificial material. c) Patterning of the photoresist mask to define the sacrificial mesa structures that will support the cantilever. d) RIE of the sacrificial material and removal of the photoresist mask. e) Blanket sputter deposition of a 30 nm Ti and 300 nm Cu seed layer and patterning the photoresist mask to define the cantilever. f) Electroplating 2 μm thick Ni-Fe and removal of the photoresist mould. g) Wet etch of the seed layer over the areas previously covered by the photoresist mask. h) Removal of the sacrificial material and release of the Ni-Fe cantilever.

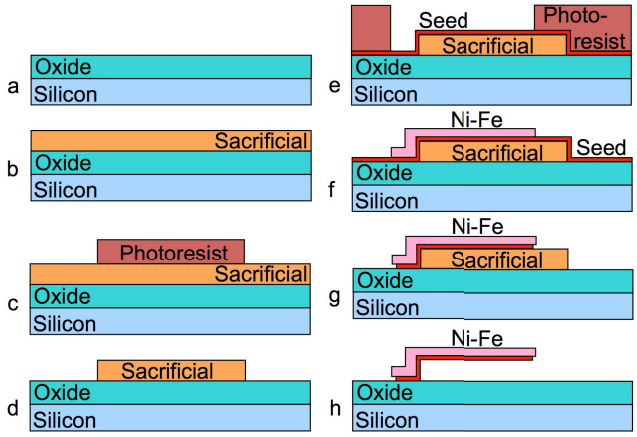

Fig. 6. Process flow for the fabrication of cantilever test structures.

The following range of materials were considered for use as the sacrificial layer, the key parameter being compatibility with the other layers used in the full switch architecture, in particular ensuring that the Ni-Fe integrity and functionality were fully preserved.

A. Parylene-C as Sacrificial Material

The test chip was initially used to determine whether Parylene-C could be used to release cantilevers with different anchor geometry, width and etch-release hole distributions, while maintaining the original process flow (Fig. 2). The release tests on the whole range of cantilever designs, however, confirmed the difficulties already reported for the full actuator. The O_2 plasma etch failed to release the cantilevers after treatment for 1 hour, and the relatively high processing temperature of around 70 °C induces progressive deterioration and stress gradient build-up. To investigate further, the etch was extended to 4 hours to monitor the effect on the suspended structures.

Fig. 7 shows that a 4-hour oxygen plasma treatment is sufficient to release cantilevers with all-around anchors of widths up to 50 μm for the designs with continuous slits and 5 $\times$ 20 μm etch holes, and up to 30 μm for the designs with 5 $\times$ 10 μm etch holes. However, this treatment proved detrimental for all the released structures, either inducing significant stress gradient that curls up the freestanding cantilevers or just visibly destroying the devices. The curling up effect is thought to be due to the oxidation of the exposed top surface of the Ni-Fe films, while the bottom surface is protected from the plasma by the sacrificial layer. Fig. 8 shows two different stress gradients observed on the same die, induced by the 4 hour oxygen plasma treatment.

The small physical distance between these two cantilevers indicates that this phenomenon is not particularly uniform and

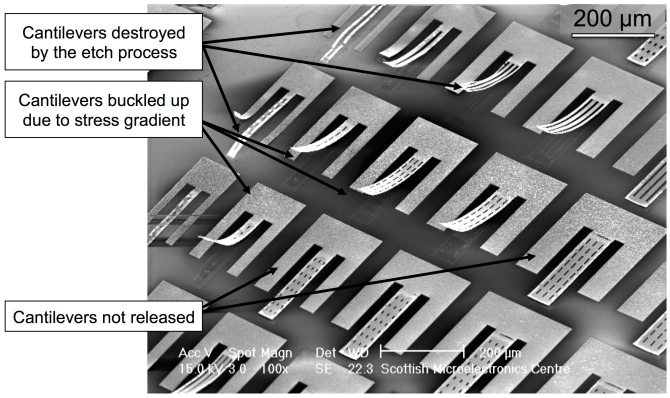

Fig. 7. Test cantilevers with all-around anchor after treatment for 4 hours in O_2 plasma.

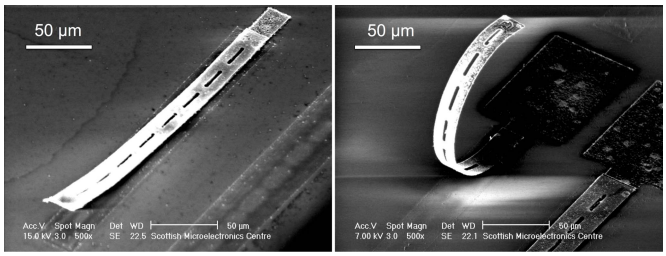

Fig. 8. Cantilevers buckling due to stress gradient in Ni-Fe.

while it can have a desirable anti-stiction effect in its milder form (left image), it can prove totally destructive in the worst cases (right image).

Clearly stress problems of the same nature as those encountered during the release of full actuator devices were observed for all the investigated design variations. This suggests that the release process is responsible for the development of the stress gradient in NiFe, which cannot be addressed by simple layout modifications.

B. Polysilicon as Sacrificial Material

To confirm whether the release process is the sole factor responsible for the development of the observed stress gradient, an alternative sacrificial material was chosen that can be patterned and etched without applying thermal loads, so as to avoid any oxidation or deterioration of the NiFe film. To this end, the tests were repeated using a second batch of test wafers with polysilicon as the sacrificial material.

The XeF_2 vapour etch process offers the advantages of being cleaner, faster and room-temperature, compared with the oxygen plasma used to remove Parylene-C. The sacrificial films were thermally deposited in a furnace, at 590 °C and although the high temperature required for the deposition makes this process incompatible with the fabrication of the complete switch device of Fig. 1, these tests were conducted with the aim of isolating the effect of thermal loads on Ni-Fe cantilevers exclusively during the release process.[1] Fig. 9 shows images of Ni-Fe cantilevers electroplated on sacrificial polysilicon mesas

[1]For the magnetic switch architecture a low temperature (<200 °C) sacrificial silicon deposition process is required.

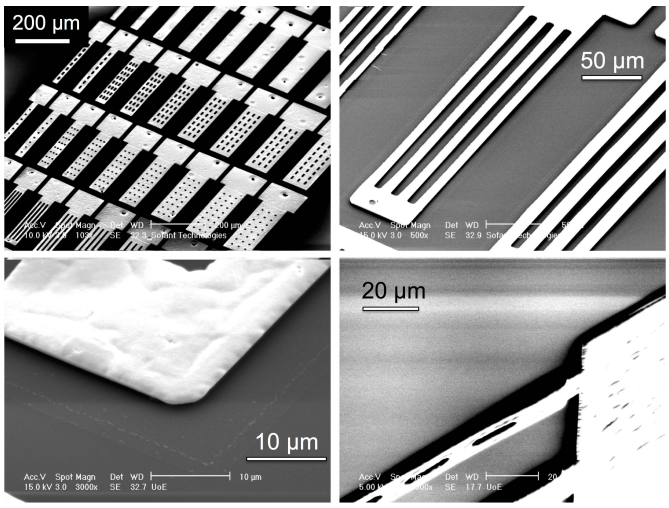

Fig. 9. SEM image of test cantilevers after 20 minutes XeF_2 etch. The polysilicon mesas are completely etched.

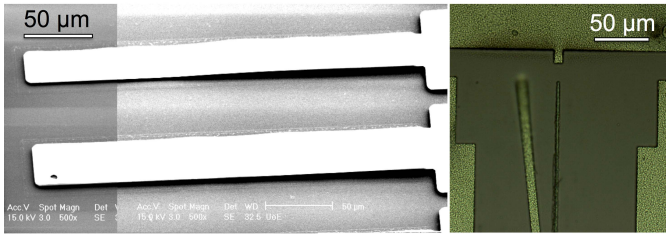

Fig. 10. Stress gradient in Ni-Fe cantilevers after removal of the polysilicon mesas. The cantilevers droop down towards the substrate (left image), while pointer arms on strain structures fabricated in the same film are curled upwards (right image).

and released after etching for only 20 minutes in the XeF_2 chamber.

Visual inspection of the test devices confirms that the XeF_2 vapour etch is a robust and clean process. The etching rate depends on the area of exposed material (including the silicon substrate if unprotected), but the process allows complete removal of the sacrificial mesas in less than 30 minutes for all the designed variations, regardless of whether whole wafers or single chips are processed. Although the etch process is neat and effective, a different structural stress problem affected all the cantilevers electrodeposited on polysilicon mesas. Every NiFe cantilever fabricated with this process drooped down towards the substrate once released, as partially visible in Fig. 9. Fig. 10 (left) illustrates this in more detail. A particularly helpful insight is given by comparing the mechanical strain observed on the cantilevers and on the suspended beams of the stress relief structures. Fig. 10 facilitates such comparison by showing that while cantilevers droop downwards (left image), the other suspended beams are curled upwards (right image).

These results demonstrate how nominally identical structures formed using the same electrodeposited Ni-Fe film can exhibit opposite out-of-plane strain. Since all thermal loads on the Ni-Fe films were eliminated by using the XeF_2 dry etch process, the factor deemed responsible for this behaviour is the anchor step, as cantilevers electroplated on sharp corners

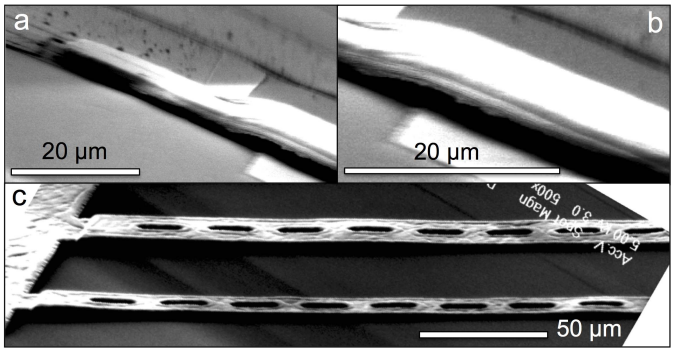

Fig. 11. Anchor points for Ni-Fe cantilevers electrodeposited on Parylene-C (a, b) and polysilicon (c) sacrificial mesas, after the release process. The images show the difference between cantilevers electroplated on the gentle slope of Parylene-C mesas compared with the steep step profile of polysilicon mesas.

droop down towards the substrate (Fig. 10 (left)), while beams electroplated on a planar surface curl upwards (Fig. 10 (right)).

C. Discussion

No drooping of the cantilever profile towards the substrate was observed during the release tests with Parylene-C as a sacrificial layer. This can be attributed to the combined effect of two factors. First, the Parylene-C mesas undergo smearing during the subsequent photolithography baking steps. This rounds the corners on the step-up to the sacrificial mesas, creating gentler slopes for the cantilever anchors. Secondly, the oxidation of the exposed Ni-Fe surface treated in the oxygen plasma used to remove the sacrificial Parylene-C induces the development of an unpredictable level of stress gradient. Fig. 11 facilitates the comparison between the observed behaviour of Ni-Fe cantilevers electroplated on the two different sacrificial mesa materials.

It was important to verify whether the oxygen plasma treatment is effectively responsible for the introduction of a stress gradient that curls the Ni-Fe cantilevers upwards, as seen for the Parylene-C tests in Fig. 8. To this end, the wafer exhibiting the drooping effect on cantilevers was treated, after the XeF_2 release etch, for 1 hour in the same oxygen plasma chamber used for the Parylene-C tests. The released devices were then examined under a Zygo white light interferometer to reconstruct the topography of the investigated surface. Fig. 12 presents a map of a sample portion of the test wafer (top image), with profile scans of two cantilevers (bottom image).

The plots clearly show that the plasma treatment reverses the drooping effect, with the cantilevers now curled upwards, contrary to the profile observed in Fig. 10 (left). The tips of the cantilevers buckle up in an unpredictable and non-uniform manner, reaching heights of more than 10 μm.

These results identify that the thermal load, with the consequent oxidation of the top surface of the Ni-Fe during surface micromachining, and the anchor step both play a crucial role in the development of stress gradient in freestanding Ni-Fe cantilevers. There is therefore a need to modify the anchor design so that it does not affect the mechanical behaviour of the cantilevers and also integrate a suitable sacrificial material that enables low-temperature deposition, patterning and complete removal.

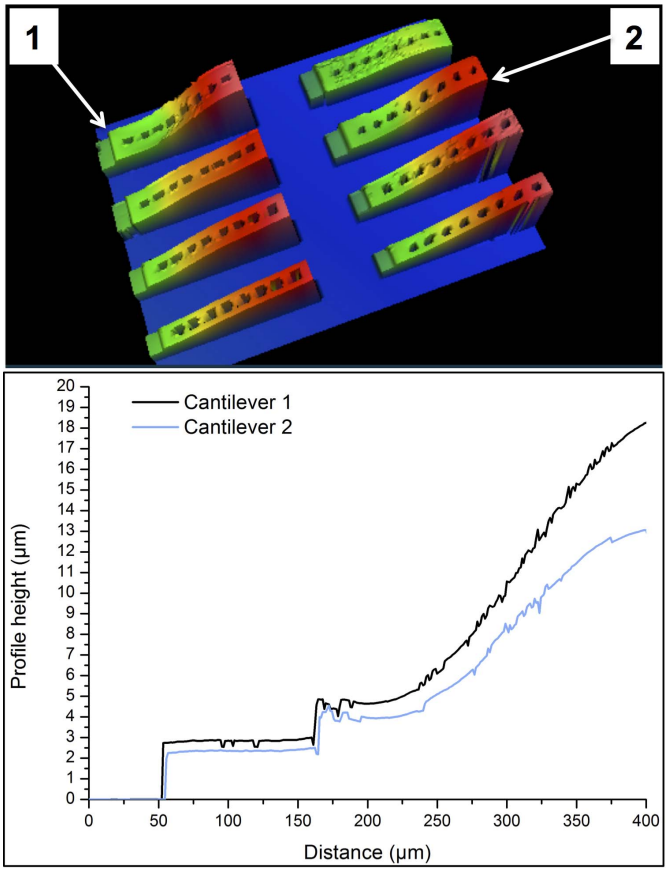

Fig. 12. White light interferometry surface maps and profile scans of Ni-Fe cantilevers on polysilicon after treatment for 1 hour in oxygen plasma. The profile curves for cantilevers 1 and 2 are taken parallel to the beam length, 10 μm from the lateral edge.

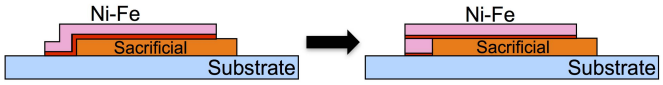

Fig. 13. Modification of the single step electroplating of a Ni-Fe cantilever to a two-step scheme.

IV. Two-Step Cantilever Electroplating

The release tests identified the need for an alternative process that avoids the stress gradient problems seen with Parylene-C and polysilicon and, at the same time, guarantees compatibility with the complete process flow of Fig. 2. A new architecture is proposed to eliminate the cantilever drooping effect resulting from the step profile on the anchor observed in the test cantilevers on polysilicon mesas. This involves electroplating in two steps, as illustrated in Fig. 13.

The advantage of this approach is that the cantilever beam is electrodeposited on the surface defined by the anchor and the sacrificial mesa, with no step-up at the joint point.

With regard to the choice of sacrificial material, Parylene-C exhibited a very low release etch rate, with the oxygen plasma causing damage to the surrounding structures during the long

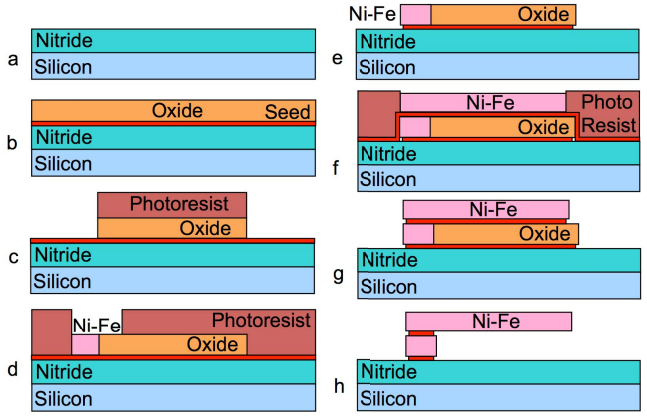

Fig. 14. Process flow for the new anchor design.

processing time. Polysilicon is a good candidate for the release process as it enables a quick etch, but the temperatures required for its thermal deposition are incompatible with the underlying SU-8 matrix. Therefore, the final sacrificial material investigated was SiO_2. Silicon dioxide deposited by means of PECVD can be patterned by RIE to define the sacrificial structures and then completely removed with a dry HF vapour etch process. The fabrication follows the process schematically illustrated in Fig. 14.

With reference to Fig. 14, the fabrication requires the following steps. a) PECVD deposition of 200 nm Si_3N_4 on a silicon substrate for insulation. Silicon nitride replaces silicon dioxide as the insulator, since SiO_2 is subsequently used as sacrificial material for surface micromachining. b) Sputter deposition of 30 nm Ti and 300 nm Cu seed layer and subsequent PECVD of $\sim$2 μm of sacrificial SiO_2. c) Photolithography and RIE patterning of SiO_2 to define the sacrificial mesa structures that support the cantilevers. d) Photoresist strip followed by photolithography to define the cantilever anchors and electrodeposition of Ni-Fe to a thickness that matches the sacrificial mesa level. e) Photoresist strip followed by wet etch of the seed layer. f) Sputter deposition of 30 nm Ti and 300 nm Cu seed layer, photolithography to define the cantilever beams and electrodeposition of Ni-Fe. g) Photoresist strip and wet etching of the seed layer. h) Removal of the sacrificial SiO_2 by vapour HF etch and wet etch of the remaining seed layer and critical point drying to avoid stiction.

The cantilever beams must be electrodeposited on a planar surface and the Ni-Fe anchors therefore need to match the step height of the sacrificial mesas. This is achieved by carefully calibrating the time of the electrodeposition. Fig. 15 illustrates the surface profile of one of the cantilever anchors, exhibiting significant surface roughness compared to the sacrificial mesa, with peaks of approximately 200 nm. Electroplating the Ni-Fe cantilever beams on this surface worked well with good adhesion. However, should a smoother surface be required, this may be achieved by optimising the electroplating bath with the addition of levellers [30], [31].

The concluding step in the fabrication of freestanding cantilevers is the complete etch of the sacrificial material by removing the remaining SiO_2 with vapour HF. The sacrificial dielectric etch process releases the cantilevers in less than

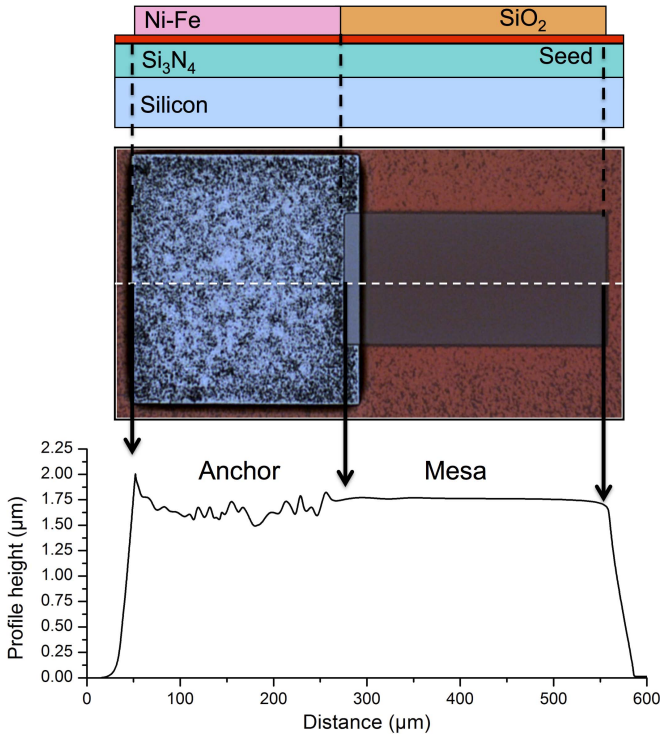

Fig. 15. Profile of an anchor electrodeposited to a thickness that matches the height of the sacrificial mesa.

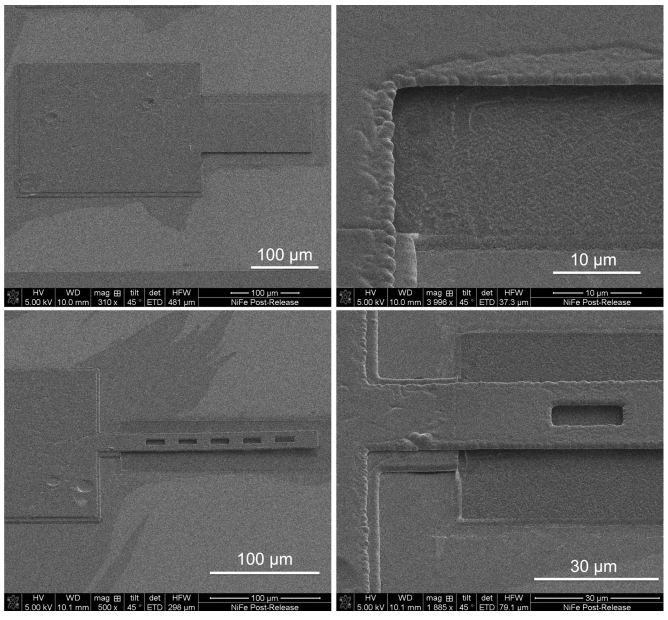

Fig. 16. SEM images of a broad solid cantilever (top) and a narrow device with etch release holes (bottom).

5 minutes without attacking the Ni-Fe structures. Fig. 16 shows suspended cantilevers of different dimensions.

This HF vapour phase process released all the cantilever geometries, including the broad solid devices as well as the narrow devices with the etch-release holes. The proposed two-step anchor process thus effectively removes any requirement for etch-release holes and enables cantilevers of all the investigated dimensions (up to 100 μm wide) to be

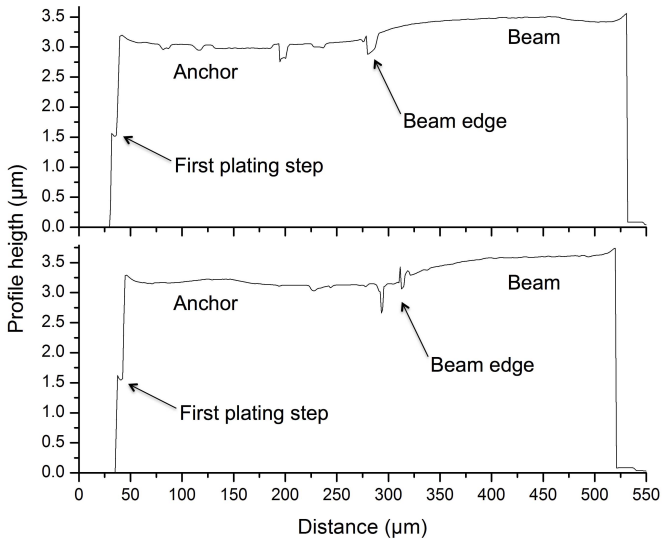

Fig. 17. Interferometry profiles of two cantilevers corresponding to the structures presented in Fig. 16: on the centreline of a broad solid cantilever, (top) and along a narrow beam with etch-release holes (bottom). The scan line for the narrow cantilever (bottom) is equidistant between the beam edge and the edges of the etch-release holes. For ease of comparison, the x axes of the two plots share the same scale.

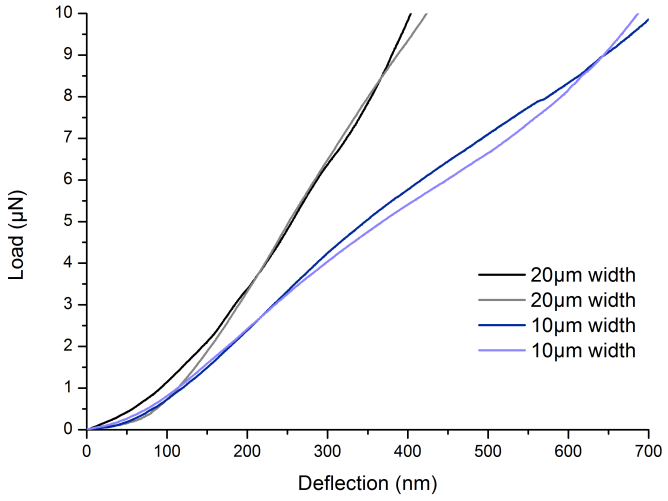

Fig. 18. Load-deflection curves for solid 10 μm and 20 μm wide cantilevers. The two curves per device indicate two repeated deflection measurements.

TABLE II
COMPARISON OF SACRIFICIAL MATERIALS AND THEIR PROCESSES

	Parylene-C	**Polysilicon**	**PECVD SiO_2**
Deposition T	✓✓ Room T	✗ 590°C	✓ < 200°C
Deposition time	✗ 4 h	✗ ~ 9 h	✓✓ ~ 1 h
Patterning T	✓✓ Room T	✓✓ Room T	✓✓ Room T
Patterning time	✓✓ ~ 25 min	✗ ~ 2 h	✓ ~ 90 min
Removal T	✗ > 70°C	✓✓ Room T	✓✓ Room T
Removal time	✗ > 4 h	✓ 20 – 30 min	✓✓ 5 min

easily released. The adoption of the proposed anchor in the magnetic MEMS switching devices enables reluctance-based cantilever actuators to be designed without sacrificing any magnetic material, thus delivering higher actuation forces.

The cantilevers appear quasi stress-free, benefiting from the stress control techniques applied during electrodeposition, as validated for blanket films and simple patterned structures [24], and avoiding any stress gradient effects introduced by the step-anchor design. The morphology of cantilevers fabricated with the new anchor design was observed by white light interferometry to verify that the beams exhibit a near horizontal profile. Fig. 17 shows profile plots of the two different cantilever designs presented in Fig. 16.

The two sample profiles in Fig. 17 show satisfactory planarity, with a maximum height variation of around 250 nm over a gap of approximately 1.6 μm (thickness of the sacrificial SiO_2) and a length of 200 μm. This is a substantial improvement over the previously described devices designed with simple anchors. The profiles highlight the interface between the first and the second electrodeposition steps (also visible around the anchors in Fig. 16), which roughly corresponds to the nominal air gap below the beams.

To validate the mechanical robustness of the devices produced, a Hysitron triboindenter tool equipped with a Berkovich diamond tip was used to exert a controlled point-load to the tip of two sample solid cantilevers. The measured deflection in response to the controlled load gives qualitative information on the stiffness of the fabricated freestanding structures and these measurements are presented in Fig. 18.

Table II offers a comparison of the tested sacrificial materials, highlighting the observed impact of the required processes on the thermal load applied before (2 μm deposition, patterning) and after (complete removal) electrodepositing the Ni-Fe cantilevers. The information summarised in the table justifies the selection of PECVD SiO_2 as best sacrificial material for applications that require materials sensitive to thermal loads such as SU-8 and Ni-Fe.

V. CONCLUSIONS

This paper has demonstrated the successful fabrication of freestanding magnetic cantilevers that are robust and do not exhibit bending effects. The stress gradient problems encountered in the initial design and process architecture have been addressed and solved by developing an alternative two-step electroplating approach. The reported solution involves a higher level of manufacturing complexity, but offers key benefits for the functionality of magnetically actuated devices. The reported final process flow offers the opportunity to rapidly release cantilevers of all the investigated dimensions. When designing magnetic actuators based on Ni-Fe cantilevers it is often necessary to select a balance between the volume ratio of magnetic material and ease of processing by incorporating etch-release holes in the design of freestanding structures. The final architecture facilitates the rapid release of solid cantilevers of widths up to 100 μm as originally designed, with no need for the inclusion of etch-release holes. This simplifies the design of the interconnect and latch layout and has the added benefit that it enables a higher volume of magnetic material to be used in reluctance-based actuators, improving the performance and facilitating the use of simpler design models for predicting the magnetic behaviour.

The final anchor design does not introduce further mechanical stress, with the suspended structures exhibiting strain

levels that match those achieved in simple patterned films with standard electrodeposition recipes [24], [25]. In light of the integration of the new anchor with the Ni-Fe cantilevers, all the required processing steps have already been demonstrated on SU-8 coated substrates as presented in section II, except for the HF vapour etch release process. However, the SU-8 layer is covered by the insulator (SiO_2 in the initial architecture, Si_3N_4 in the final architecture) and metal (Al) layers both in the initial and final architectures, and is thus not exposed to any surface chemical action. By avoiding any thermal loads during surface micromachining, the final process can therefore be considered compatible with fabrication on polymer substrates (e.g. SU-8) as originally intended for embedded actuation coils.

REFERENCES

[1] A. J. Strojwas, "Conquering process variability: A key enabler for profitable manufacturing in advanced technology nodes," in *Proc. IEEE Int. Symp. Semicond. Manuf. (ISSM)*, Sep. 2006, pp. 23–32. [Online]. Available: http://ieeexplore.ieee.org/xpls/abs_all.jsp?arnumber=4493000

[2] J. K. Luo, M. Pritschow, A. J. Flewitt, S. M. Spearing, N. A. Fleck, and W. I. Milne, "Effects of process conditions on properties of electroplated Ni thin films for microsystem applications," *J. Electrochem. Soc.*, vol. 153, no. 10, pp. D155–D161, Jul. 2006. [Online]. Available: http://jes.ecsdl.org/content/153/10/D155

[3] Y.-H. Zhang, G.-F. Ding, Y.-L. Cai, H. Wang, and B. Cai, "Electroplating of low stress permalloy for MEMS," *Mater. Characterization*, vol. 57, no. 2, pp. 121–126, Aug. 2006. [Online]. Available: http://www.sciencedirect.com/science/article/pii/S104458030600009X

[4] A. B. Horsfall *et al.*, "Dependence of process parameters on stress generation in aluminum thin films," *IEEE Trans. Device Mater. Rel.*, vol. 4, no. 3, pp. 482–487, Sep. 2004. [Online]. Available: http://ieeexplore.ieee.org/xpl/articleDetails.jsp?arnumber=1369210

[5] L. Daniel, C. R. Sullivan, and S. R. Sanders, "Design of microfabricated inductors," in *Proc. 27th Annu. IEEE Power Electron. Spec. Conf. (PESC)*, Jun. 1996, pp. 1447–1455. [Online]. Available: http://ieeexplore.ieee.org/xpls/abs_all.jsp?arnumber=548772

[6] C. R. Sullivan and S. R. Sanders, "Design of microfabricated transformers and inductors for high-frequency power conversion," *IEEE Trans. Power Electron.*, vol. 11, no. 2, pp. 228–238, Mar. 1996. [Online]. Available: http://ieeexplore.ieee.org/xpl/articleDetails.jsp?arnumber=486170

[7] D. Flynn and M. P. Y. Desmulliez, "Influence of pulse reverse plating on the properties of Ni-Fe thin films," *IEEE Trans. Magn.*, vol. 46, no. 4, pp. 979–985, Apr. 2010. [Online]. Available: http://ieeexplore.ieee.org/xpls/abs_all.jsp?arnumber=5339220

[8] K. I. Arai and T. Honda, "Micromagnetic actuators," *Robotica*, vol. 14, no. 5, pp. 477–481, 1996. [Online]. Available: http://journals.cambridge.org/action/displayAbstract?fromPage=online&aid=4529228

[9] D. Niarchos, "Magnetic MEMS: Key issues and some applications," *Sens. Actuators A, Phys.*, vol. 106, nos. 1–3, pp. 255–262, Sep. 2003. [Online]. Available: http://www.sciencedirect.com/science/article/pii/S0924424703001791

[10] R. Girard, "The electrodeposition of thin magnetic permalloy films," *J. Appl. Phys.*, vol. 38, no. 3, pp. 1423–1430, Mar. 1967. [Online]. Available: http://scitation.aip.org/content/aip/journal/jap/38/3/10.1063/1.1709651

[11] S. E. Hadian and D. R. Gabe, "Residual stresses in electrodeposits of nickel and nickel–iron alloys," *Surf. Coat. Technol.*, vol. 122, nos. 2–3, pp. 118–135, Dec. 1999. [Online]. Available: http://www.sciencedirect.com/science/article/pii/S025789729900328X

[12] M. M. Yang and J. A. Aboaf, "RF-diode sputtered Permalloy film," *J. Appl. Phys.*, vol. 66, no. 8, pp. 3734–3740, Oct. 1989. [Online]. Available: http://scitation.aip.org/content/aip/journal/jap/66/8/10.1063/1.344059

[13] W. P. Taylor, O. Brand, and M. G. Allen, "Fully integrated magnetically actuated micromachined relays," *J. Microelectromech. Syst.*, vol. 7, no. 2, pp. 181–191, Jun. 1998. [Online]. Available: http://ieeexplore.ieee.org/xpls/abs_all.jsp?arnumber=679353

[14] W. P. Taylor and M. G. Allen, "Integrated magnetic microrelays: Normally open, normally closed, and multi-pole devices," in *Proc. Int. Conf. Solid-State Sens. Actuators (TRANSDUCERS)*, Jun. 1997, pp. 1149–1152. [Online]. Available: http://ieeexplore.ieee.org/stamp/stamp.jsp?arnumber=00635408

[15] M. Ruan, J. Shen, and C. B. Wheeler, "Latching micromagnetic relays," *J. Microelectromech. Syst.*, vol. 10, no. 4, pp. 511–517, Dec. 2001. [Online]. Available: http://ieeexplore.ieee.org/xpls/abs_all.jsp?arnumber=967373

[16] I.-J. Cho, T. Song, S.-H. Baek, and E. Yoon, "A low-voltage and low-power RF MEMS series and shunt switches actuated by combination of electromagnetic and electrostatic forces," *IEEE Trans. Microw. Theory Techn.*, vol. 53, no. 7, pp. 2450–2457, Jul. 2005. [Online]. Available: http://ieeexplore.ieee.org/xpls/abs_all.jsp?arnumber=1463370

[17] I.-J. Cho and E. Yoon, "Design and fabrication of a single membrane push-pull SPDT RF MEMS switch operated by electromagnetic actuation and electrostatic hold," *J. Micromech. Microeng.*, vol. 20, no. 3, p. 035028, Mar. 2010. [Online]. Available: http://iopscience.iop.org/0960-1317/20/3/035028/

[18] M. Glickman, P. Tseng, J. Harrison, T. Niblock, I. B. Goldberg, and J. W. Judy, "High-performance lateral-actuating magnetic MEMS switch," *J. Microelectromech. Syst.*, vol. 20, no. 4, pp. 842–851, Aug. 2011. [Online]. Available: http://ieeexplore.ieee.org/xpl/articleDetails.jsp?arnumber=5948315

[19] G. D. Gray, Jr., and P. A. Kohl, "Magnetically bistable actuator: Part 1. Ultra-low switching energy and modeling," *Sens. Actuators A, Phys.*, vol. 119, no. 2, pp. 489–501, Apr. 2005. [Online]. Available: http://www.sciencedirect.com/science/article/pii/S0924424704007794

[20] G. D. Gray Jr., E. M. Prophet, L. Zhua, and P. A. Kohl, "Magnetically bistable actuator: Part 2. Fabrication and performance," *Sens. Actuators A, Phys.*, vol. 119, no. 2, pp. 502–511, Apr. 2005. [Online]. Available: http://www.sciencedirect.com/science/article/pii/S0924424704007800

[21] S. Fu, G. Ding, H. Wang, Z. Yang, and J. Feng, "Design and fabrication of a magnetic bi-stable electromagnetic MEMS relay," *Microelectron. J.*, vol. 38, nos. 4–5, pp. 556–563, Apr./May 2007. [Online]. Available: http://www.sciencedirect.com/science/article/pii/S0026269207000547

[22] G. M. Rebeiz, "RF MEMS switches: Status of the technology," in *Proc. 12th Int. Conf. Solid-State Sens., Actuators, Microsyst. (TRANSDUCERS)*, vol. 2. Jun. 2003, pp. 1726–1729. [Online]. Available: http://ieeexplore.ieee.org/xpls/abs_all.jsp?arnumber=1217118

[23] G. M. Rebeiz, *RF MEMS—Theory, Design and Technology*. Hoboken, NJ, USA: Wiley, 2003.

[24] J. Murray, G. Schiavone, S. Smith, J. Terry, A. R. Mount, and A. J. Walton, "Characterisation of electroplated NiFe films using test structures and wafer mapped measurements," in *Proc. IEEE Int. Conf. Microelectron. Test Struct. (ICMTS)*, Apr. 2011, pp. 63–68. [Online]. Available: http://ieeexplore.ieee.org/xpls/abs_all.jsp?arnumber=5976861

[25] G. Schiavone *et al.*, "Quantitative wafer mapping of residual stress in electroplated NiFe films using independent strain and Young's modulus measurements," in *Proc. IEEE Int. Conf. Microelectron. Test Struct. (ICMTS)*, Apr. 2012, pp. 105–110. [Online]. Available: http://ieeexplore.ieee.org/xpls/abs_all.jsp?arnumber=6190629

[26] G. Schiavone, S. Smith, J. Murray, J. G. Terry, M. P .Y. Desmulliez, and A. J. Walton, "Micromechanical test structures for the characterisation of electroplated NiFe cantilevers and their viability for use in MEMS switching devices," in *Proc. IEEE Int. Conf. Microelectron. Test Struct. (ICMTS)*, Mar. 2013, pp. 13–18. [Online]. Available: http://ieeexplore.ieee.org/xpl/articleDetails.jsp?arnumber=6528138

[27] R. Walker *et al.*, "Characterisation and integration of Parylene as an insulating structural layer for high aspect ratio electroplated copper coils," in *Proc. IEEE Int. Conf. Microelectron. Test Struct. (ICMTS)*, Mar. 2013, pp. 7–12. [Online]. Available: http://ieeexplore.ieee.org/xpl/articleDetails.jsp?arnumber=6528137

[28] R. Walker *et al.*, "Characterisation of residual stress in dielectric films studied by automated wafer mapping," in *Proc. IEEE Int. Conf. Microelectron. Test Struct. (ICMTS)*, Mar. 2014, pp. 98–103. [Online]. Available: http://ieeexplore.ieee.org/xpl/articleDetails.jsp?arnumber=6841475

[29] S. Smith *et al.*, "Fabrication and measurement of test structures to monitor stress in SU-8 films," *IEEE Trans. Semicond. Manuf.*, vol. 25, no. 3, pp. 346–354, Aug. 2012. [Online]. Available: http://ieeexplore.ieee.org/xpl/articleDetails.jsp?arnumber=6212378

[30] W. Bang and K. Hong, "Planarity improvement and reduction of coercivity by organic additives in electroplated Ni–Fe permalloy thin films," *Electrochem. Solid-State Lett.*, vol. 10, no. 8, pp. J86–J88, May 2007. [Online]. Available: http://esl.ecsdl.org/content/10/8/J86.abstract?related-urls=yes&legid=esl;10/8/J86

[31] W. Bang, J. B. Lee, K. Hong, Y.-D. Ko, J.-S. Chung, and H. Lee, "Permeability change of electroplated Ni–Fe permalloy thin films by a leveller added to the electrolyte," *Phys. Status Solidi A*, vol. 204, no. 12, pp. 4067–4070, Dec. 2007. [Online]. Available: http://onlinelibrary.wiley.com/doi/10.1002/pssa.200777321/abstract

Giuseppe Schiavone was born in Bitonto, Italy, in 1985. He received the B.Eng. degree in physical engineering and the M.Sc. degree in micro and nanotechnologies from the Politecnico di Torino, Turin, Italy, in 2007 and 2009, respectively; the M.Sc. degree in micro and nanoelectronics from Univérsité Joseph Fourier, Grenoble, France, in 2009; and the Ph.D. degree in magnetic microelectromechanical systems from the School of Engineering, University of Edinburgh, Edinburgh, U.K., in 2014.

He is currently a Research Associate with the Research Institute of Signals, Sensors, and Systems, School of Engineering and Physical Sciences, Heriot-Watt University, Edinburgh.

Andrew S. Bunting received the B.Sc. (Hons.) degree in physics from the University of St. Andrews, St. Andrews, U.K., in 1991, and the Ph.D. degree from the University of Glasgow, Glasgow, U.K., in 1996, with a thesis entitled Characterisation of Reactive Ion Etch Processes for Ternary III-V Semiconductors.

He held engineering positions with Raytheon Systems and Alcatel Optronics, and is currently a Research Fellow with the School of Engineering, University of Edinburgh, Edinburgh, U.K. His main research interests lie with the development of microfabrication processes for novel sensors and post-processing on CMOS.

Marc P. Y. Desmulliez (M'08–SM'12) was born in Lille, France, in 1963. He received the degree from the École Supérieure d'Électricité of Paris, Paris, France, in 1987; the dual Diploma degrees in microwave and modern optics, and theoretical physics from University College London, London, U.K., and the University of Cambridge, Cambridge, U.K., in 1987 and 1989, respectively; and the Ph.D. degree in optoelectronics from Heriot-Watt University, Edinburgh, U.K., in 1995.

He is currently the Head of the Research Institute of Signals, Sensors, and Systems with the School of Engineering and Physical Sciences, Heriot-Watt University, where he has been the Director of the Microsystems Engineering Centre since 1999.

Prof. Desmulliez is a Fellow of the Institute of Engineering and Technology and the Institute of Physics. He is also a Chartered Engineer and a Chartered Physicist of the Institute of Physics, U.K.

Anthony J. Walton (SM'88) is currently a Professor of Microelectronic Manufacturing with the School of Engineering, Scottish Microelectronics Centre, University of Edinburgh, Edinburgh, U.K. Over the past 25 years, he has been actively involved with the semiconductor industry in a number of areas associated with silicon processing. These include integrated circuit technology, microsystems and the development of technologies, and their integration with CMOS. He played a key role in setting up the Scottish Microelectronics Centre, which is a purpose-built facility for research, development, and commercialization. He has authored over 350 papers.

Prof. Walton was a recipient of the Best Paper Award for the IEEE TRANSACTIONS ON SEMICONDUCTOR MANUFACTURING, the *Proceeding of the International School of Hydrocarbon Measurement*, and the IEEE International Conference on Microelectronic Test Structures (ICMTS) in 2004, and the IET Nanobiotechnology Premium Award in 2007. He has served as the Chairman of a number of conferences, which include the European Solid-State Devices Research Conference in 1994 and 2008, and ICMTS in 1989 and 2008. He also serves on numerous technical committees and is an Associate Editor of the IEEE TRANSACTIONS ON SEMICONDUCTOR MANUFACTURING.